PHYSICAL REVIEW A VOLUME 24, NUMBER 4 OCTOBER 1981

Optical bistability by an atomic vapor in a focusing Fabry-Perot cavity

W. J. Sandle*
Physics Department, University of Otago Dunedin, New Zealand

Alan Gallagher[†]
Joint Institute for Laboratory Astrophysics, National Bureau of Standards and University of Colorado, Boulder, Colorado 80309
(Received 24 March 1980; revised manuscript received 18 May 1981)

We report experimental observations of dispersive- and absorptive-optical bistability due to saturation of the D_1 line of atomic sodium in a tight-focused Fabry-Perot cavity. Under the conditions of large optical power broadening and substantial collisional broadening by argon buffer gas used for part of the data, the sodium very nearly behaves as a two-level homogeneously broadened absorber. It thus yields a test of the two-level mean-field optical-bistability model. That model, including homogeneous broadening, fails to account quantitatively for the power levels and power dependencies of the cavity transmission. In particular, this model predicts too rapid an onset of atomic saturation with cavity power. In contrast, predictions of a two-level Gaussian-field optical-bistability model for the dependence of transmitted power as a function of laser power and frequency are confirmed by the experimental data. However, there is a remaining discrepancy in the absolute value of the cavity power.

I. INTRODUCTION

A history and review of work in optical bistability can be found in Refs. 1 and 2 and the references therein. The topic has attracted considerable interest since the first convincing demonstration by Gibbs, McCall, and Venkatesan[3] of the existence of more than one transmitting state for a Fabry-Perot etalon containing a nonlinear dispersive and absorptive medium. Much of this interest has been theoretical, and the simple model developed by Bonifacio and Lugiato[4-6] of two-level homogeneously broadened absorbers in a plane-wave ring optical cavity has assumed an important role. However, of the optical-bistability experiments so far, none has been primarily concerned with providing comparison with this simple model in which the nonlinearity is due to saturation of a homogeneously broadened two-level transition.[7] This communication reports such a comparison, using an atomic vapor in which the characteristics of the absorber are well understood.

Our experiment resembles that of Gibbs *et al.*[3] in utilizing the D_1 line of atomic sodium as the absorber inside a Fabry-Perot etalon. However, the emphasis is quite different in the two cases. Their emphasis was on reporting observations of dispersive-optical bistability under conditions where hyperfine pumping between the ground state $F=1$ and 2 levels at low laser-power levels provided nonlinearity in the index of refraction n. Absorptive bistability was also seen, at the highest laser powers, at one of the three frequencies where optical pumping did not alter n. The relative importance of two-level saturation versus optical pumping in those observations is not discussed. In contrast, the present experiment involves predominantly two-level saturation effects at high laser powers.

We have utilized slow scanning of the laser frequency to obtain the steady-state relations between input and transmitted power. In part of the experiment the laser was scanned across many widths of the sodium transition, and there were many narrow cavity resonances within the width of the sodium transition. Other more rapid scans were made across individual cavity resonances. In this manner we have observed switching and hysteresis for dispersive bistability off the atomic resonance and absorptive bistability on resonance. In the following we will first discuss the simple model, then the details and results of the experiments, followed by comparisons to the model and our conclusions.

II. APPLICATION OF THE TWO-LEVEL MEAN-FIELD HOMOGENEOUS MODEL

In the two-level, mean-field homogeneous (TMH) model all absorbers are assumed to be two level, to have the same resonant frequency, and to experience the same (mean) field,[6,8-10] which requires low single-pass absorption and high cavity finesse. For small laser-cavity detuning, this model yields[5,11,12] the optical-bistability state equation

$$y^2=x^2\left[\left(1+\frac{2C}{1+\Delta^2+x^2}\right)^2+\left(\phi-\frac{2C\Delta}{1+\Delta^2+x^2}\right)^2\right]. \qquad (1)$$

The physical meanings of the quantities are as follows: y and x represent, respectively, the incident and transmitted optical-field amplitudes; the cooperativity factor C is a measure of the strength of the coupling between the ensemble of two-level absorbers and the cavity field; and Δ and ϕ are proportional to the laser-frequency detunings from, respectively, the two-level resonance frequency and the nearest empty optical-cavity resonance frequency.

Equation (1) was developed, without detunings in Ref. 4 and with detunings in Refs. 5 and 11, for an ideal-plane ring cavity in which the field amplitude was spatially constant. The field amplitude is not spatially constant in the present experiments since there are large microscopic variations due to the standing waves in a linear cavity, and, in addition, the absorbers are near the center of a nearly spherical Fabry-Perot cavity, where the field amplitude is Gaussian in the off-axis dimensions as well as showing some variation in the axial direction. These differences from the single field-amplitude case will be discussed further in Sec. V, in the context of comparisons between the experimental results and Eq. (1). For the purpose of applying the model we shall assume that the field in the cavity is a constant *effective field*, related in magnitude to the actual field distribution as discussed below.

In the present experiment the mirrors have unequal reflectivities and there are nonsaturable losses in the mirrors and vacuum windows, but this need not alter Eq. (1) if x and y are defined in terms of the incident and transmitted fields as follows (see Appendix A for details). The quantity y is defined in terms of the (assumed constant) *effective cavity field* that would be produced by the input field if the cavity were empty of absorbers and at resonance with respect to incident laser light. Following Ref. 12, the numerical value of y is then defined as the ratio of this particular effective cavity field amplitude to the saturation field amplitude. (The latter is the effective cavity field amplitude which when applied at the two-level resonance frequency reduces the two-level absorption by a factor of 2.) The quantity x is defined in terms of the actual *effective cavity field* under the conditions of the experiment, and the numerical value of x is the ratio of this field amplitude to the saturation field amplitude. This cavity field times the output mirror transmission coefficient is, of course, the transmitted field amplitude (adjusted to take account of cavity focusing). With these definitions

$$C = \alpha F L / 2\pi , \tag{2}$$

where L is the length of absorbers, F is the cavity finesse (without absorbers), and α is the unsaturated resonance absorption coefficient $(\lambda^2 N\Gamma/4\pi\gamma_\perp)$ of the absorbers when treated as homogeneously broadened two-level atoms with a radiative decay Γ, a homogeneous half-width at half-height $\gamma_\perp = (\Gamma/2) + (\gamma/2)$, and a collisional-broadening rate γ of ~20 MHz per Torr of Ar.[13] The detuning Δ is expressed in units of the homogeneous half-width $\gamma_\perp$ for the unsaturated two-level absorption coefficient, and ϕ is in units of the empty cavity resonance half-width, as, for example, in Ref. 5.

As described in Appendix A, the cavity gain, beam-waist size, and output mirror transmission must be measured in order to relate the axial cavity field at the beam waist to the laser and transmitted powers. The axial values of x and y are then given by the ratio of the axial field (respectively, with and without absorbers) to the saturation field. The result of Eqs. (A1)–(A4) and the experimental parameters are

$$y^2 = \frac{B\Gamma P_L}{2\gamma_\perp} , \tag{3}$$

where P_L is the laser power and $B = 4500$ for P_L expressed in mW. The mean-field value of y^2 at the waist, defined in Appendix A, is one-half of this value.

There are two experimental factors that reduce the effective axial field below this value. First, the Na fills a length of ~5 cm to each side of the beam waist, while the Rayleigh length in which the beam diameter increases by $\sqrt{2}$ is ~3.4 cm. This results in an average axial power of $\sim\frac{2}{3}$ that at the waist. Next, not all of the laser power is coupled into the axial mode of the cavity, resulting typically in a power reduction of ~20%. The effective axial value of y^2 is thus given by Eq. (3) with $B \simeq 2400$, and the effective mean-field value is half the effective axial value.

One further factor can act to reduce the value of y^2. At a buffer gas pressure of ~5 Torr, excitation transfer occurs between the $3^2P_{1/2}$ and $3^2P_{3/2}$ states at a rate comparable to Γ.[14] Since the $3^2P_{3/2}$ and $3^2P_{1/2}$ states both radiate back to the $3^2S_{1/2}$ state at the same rate and the mixing is slow compared to Γ for buffer gas pressures much smaller than 5 Torr, this excitation transfer has a minor effect on our 0.7-Torr data. For our 80-Torr data, on the other hand, the $3^2P_{1/2}$ and $3^2P_{3/2}$ states quickly attain an approximately statistical ratio, and we show in Appendix B that in this high-pressure limit one retrieves effectively two-level saturation behavior with linearly polarized excitation, but with x^2 and y^2 reduced to $\frac{2}{3}$ of their values calculated without collisional transfer. Thus, for our 80-Torr data we will use Eq. (3) with $B \simeq 1600$ (effective axial value) or 800 (effective mean-field value).

By comparing x^2 to Δ^2 in the denominator of Eq. (1), one notes that the effectiveness of detuning depends on the laser intensity. This is essentially power broadening, and it is clear that it can introduce homogeneous character into an initially inhomogeneous line. Specifically, for $x^2 = \Delta^2$, we find that $\Delta\nu_B^2 = \Omega_A^2 \gamma_\perp / \Gamma$, where Ω_A is the Rabi frequency and we will call $2\Delta\nu_B$ the power-broadened width of the line. This broadening mechanism will, of course, be present to a different degree before and after bistable switching, and indeed its role cannot be separated from the switching process itself in solutions of the bistability equations. Nonetheless, it is a quite valuable concept when applied carefully and it can clarify the importance of inhomogeneities in various features of the observations.

III. EXPERIMENT

In choosing a suitable system to test the above model, we sought an atom with a homogeneously broadened transition that can be represented as two level, and for which there is sufficient laser power to strongly saturate the transition. A transition from $J=\frac{1}{2}$ to $J=\frac{1}{2}$ levels has been shown[15-16] to behave formally as two level under steady linearly polarized excitation (see also Appendix B). We are, for these reasons, led to employ the $D_1(3^2S_{1/2} - 3^2P_{1/2})$ transition of atomic sodium. We have introduced Ar buffer gas to homogeneously broaden the initially Doppler- and hyperfine-broadened transition. The laser-power requirements for saturating the transition then must be kept in mind because the saturation intensity scales as the homogeneous half-width (see, e.g., Ref. 4), and for this reason the Na vapor is located at the waist region of a tight-focused near-concentric cavity mode, matched to a cw dye laser (see Fig. 1).

We have used a cavity constructed from mirrors of 30-cm radius of curvature and with an optical length of ~59.2 cm, determined from the frequency of off-axis modes, yielding an 80-μm spot size at the waist and a Rayleigh length of 3.4 cm. The transmission coefficients of the input and output mirrors are 1.4 and 0.8%, respectively, and the measured cavity finesse (observed far off the Na resonance) is 55. The laser is isolated from the cavity and matched into the axial cavity mode. The intracavity window and end mirror losses reduce the cavity power gain (far off the Na resonance) to 4.3. This value (obtained from transmitted power with and without the entrance mirror) is

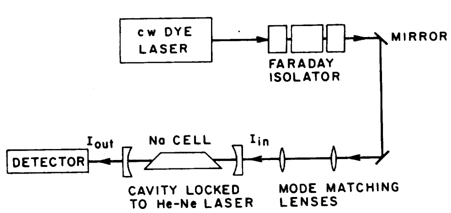

FIG. 1. Experimental arrangement.

consistent, to within 10%, with the value calculated from the measured finesse and input mirror transmission [Eqs. (A14) and (A15)].

The Na vapor is expected to fill a total of ~10 cm at the center of the cavity, and is confined by Ar buffer gas (0.2–80 Torr) in a heated tube (~150 °C) with cold Brewster windows (Fig. 1). This stainless-steel tube oven was designed for use in a double heat-pipe mode at Na densities near 1 Torr; consequently, at the lower Na densities of these experiments the Na vapor distribution was somewhat uncertain. The consequences of this uncertainty are discussed in Sec. V.

The intensity transmitted by the cavity was measured by a photomultiplier and recorded by either of two methods. In the early stages of the experiment the frequency sweep across the entire line took minutes, the cavity length was stabilized to a stable He-He laser, and the transmission was recorded on an xy recorder. Later, to obtain high powers the cavity length stablization was removed, the laser was swept in a fraction of a second, and oscilloscope traces of the cavity transmission were photographed. The line center is identified from the shape of the cavity transmission peaks, so that pressure shifts are automatically taken into account.

IV. SIGNIFICANCE OF OPTICAL PUMPING

Hyperfine optical-pumping transfers population between the two ground-state F levels of sodium, and thereby changes the relative contributions to the resonant optical absorption and index of refraction arising from each of these partially resolved hyperfine transitions (see Ref. 3 for details). The relaxation time for restoring a statistical ratio of F-state populations by collisions is generally much longer than the $3P$-state radiative lifetime, so that optical-pumping effects normally dominate over saturation effects at low powers. For the following reasons the present experiments, as opposed to those analyzed in Ref. 3, were carried out under conditions where optical-pumping effects were generally masked by saturation of the $3S$-$3P$ transition.

(1) Owing to the approximate equality of the Na Doppler width and hyperfine splitting, (hfs) the change in index of refraction n resulting from hyperfine pumping is approximately 10% or less of $n-1$, whereas saturation of the optical transition causes up to 100% changes in $n-1$. Thus, the critical atom density for bistability based on saturation is lower than for that based on pumping, and densities between these will allow saturation phenomena to be emphasized.

(2) If a small laser spot is used, each atom spends a relatively small time in the illuminated

region undergoing pumping, so that the optical-pumping threshold powers are raised. In the present experiment the beam *diameter* is less than 200 μm, averaged over the illuminated length of the vapor, and for buffer gas pressures below 1 Torr the characteristic transit time is 25 excited-state lifetimes. As ~2 optical excitations are necessary to transfer population between F levels, there is only a factor of ~12 between the characteristic saturation power and optical-pumping power under these circumstances.

(3) At higher buffer gas pressures (1–50 Torr), the dwell time in the laser spot is longer, and optical-pumping effects will show up in a low power regime separated from saturation effects. The importance of optical pumping will then depend on atom density as discussed in (1).

(4) At still higher buffer gas pressures (>50 Torr), Lorentzian pressure broadening will reduce the difference in absorption coefficients for different hyperfine components and will reduce the change of refractive index with residual pumping to less than 10% of $n-1$.

(5) At high laser powers, the power broadening of the optical transitions can greatly exceed the Na hfs splitting, so that hyperfine pumping becomes unimportant. This broadening differs considerably between the transmitting and nontransmitting state of the cavity, and the need to include Doppler as well as hyperfine inhomogeneous broadening for the low transmitting state is then an intrinsic complication of the theory. Nonetheless, power broadening can allow Fabry-Perot transmission peak heights, and other phenomena related to the high cavity-power conditions, to be validly interpreted in terms of a single, homogeneously broadened two-level transition.

(6) Each hyperfine line is a Voigt profile, with Lorentzian wings equivalent to those that would result from all atoms centered at the resonant frequency. The transition from Gaussian to Lorentzian wings of the entire absorption line occurs at $|\Delta\nu| \simeq 5$ GHz on either side of the centroid (or closer if the line is collisionally broadened). Consequently, for $|\Delta\nu| \gtrsim 5$ GHz the fractional change in $n-1$ due to optical pumping decreases as for case (5).

(7) Absorptive bistability based on optical pumping requires zero refractive-index change. None of the three frequencies[3] at which this can result from hyperfine pumping coincides with the centroid of the line, where zero refractive-index change based on saturation occurs. Bistability at these frequencies based on optical pumping requires higher laser power, and this will generally cause some saturation and thereby some index of refraction change. Thus, none of these three bistable switchings can be classed as pure absorptive.

V. RESULTS AND DISCUSSION

All results are in terms of power transmitted by the cavity as a function of laser frequency for *fixed* laser power. The results are given in four parts as follows:

(A) In the first part, an overview, showing a number of scans of the entire D_1 absorption line, as it appears probed by Fabry-Perot profiles, for the various experimental regimes determined by laser power and collisional broadening, is given.

(B) In the second, examples of individual Fabry-Perot profiles illustrating dispersive- and absorptive-optical bistability are given. The emphasis here is on the phenomenology of the switching and hysteresis seen with frequency tuning.

(C) In the third, complete scans over the D_1 absorption line are given, as for Sec. V A but where the conditions are chosen to validate many assumptions of the TMH model. Quantitative comparison between experiment and the predictions of the TMH model are made.

(D) In the fourth, the data in Sec. V C are compared to a model that accounts for the transverse Gaussian power envelope of the fundamental cavity mode.

A. Overview

The D_1 absorption line is typically ~3 GHz in width, while individual Fabry-Perot profiles are separated by a free spectral range of 250 MHz. Thus, a scan across the entire D_1 line will show a number of cavity transmission peaks whose height depends on the atomic absorption and whose position depends on the atomic dispersion.

Figure 2 shows data at low buffer gas pressure (0.7-Torr Ar, giving $\gamma_\perp = \Gamma/2 + \gamma_{\rm collis}/2 \simeq 12$ MHz), low Na density (7×10^9 cm^{-3}), and two laser powers (0.3 and 1 μW incident on the cavity). The data are presented as points at the peak of each Fabry-Perot transmission peak. The hfs associated with the D_1 line is apparent. Hyperfine pumping is negligible in the lower power curve (dots), due to the rapid transit-time relaxation (~0.4 μsec). From the data and the known cavity finesse we obtain the optical thickness (and hence αL). If we assume the Na is uniformly distributed over a 10-cm length, this corresponds to an Na density, a factor of approximately 8 below that predicted by the equilibrium vapor pressure at the cell heater temperature. Since thermal contact from the heater to the Na was rather poor (see Sec. III) and sodium evolution at the center of the cell diffuses toward

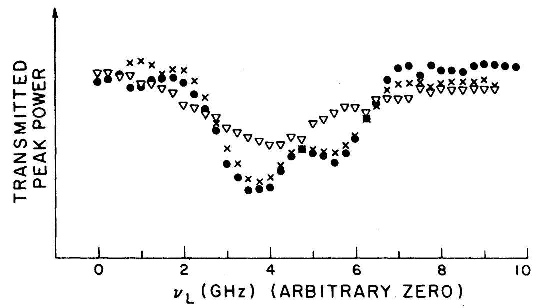

FIG. 2. Transmitted cavity power as a function of laser frequency for low laser power and low Na density (7×10^9 cm^{-3}), illustrating the low power absorption profile of the D_1 line. The data are shown as Fabry-Perot peak transmissions. Dots: laser power 0.3 μW, Ar pressure 0.7 Torr; crosses: laser power 1 μW, Ar pressure 0.7 Torr; triangles: laser power 1 μW, Ar pressure 90 Torr. These data sets have been normalized to indicate the same peak transmission signals in the far wings.

the ends, this could easily occur. Also, at low Na densities in an intermittently sealed-off cell, as used here, the Na vapor pressure does not necessarily attain its equilibrium value, even directly above the Na metal surface.

In order to obtain an estimate of αL at higher cell temperatures, where most of the measurements were taken, we assume that αL is proportional to the Na vapor density at the heater temperature. In fact, analysis of this higher temperature data provides best-fit values of αL that are consistent with this assumption provided the Na density reduction from the equilibrium value is taken as five (rather than eight).

The crosses in Fig. 2 are taken under the same conditions, except that the laser power has been raised by a factor of ~3 to 1 μW. These data have been normalized in the far wings to the lower laser-power data, so that the slight decrease in absorption in the hyperfine lines can be seen. This decrease is due to a small amount of optical pumping, and confirms that optical pumping is very minor in the lower power data. The triangles in Fig. 2 were taken at the same 1-μW power but 90-Torr Ar pressure. The diffusion time across the beam is now about 500 radiative lifetimes, and the effect of optical pumping and Lorentzian broadening is evident in the absence of hyperfine structure. For 1-μW laser power this transition to an optically pumped line shape occurs at a few Torr Ar pressure. By 90 Torr, the effect of collisional broadening can be seen in the wings in Fig.2 ($2\gamma_\perp = 1800$ MHz).

Figure 3 differs from Fig. 2 in that the laser power (60 mW) and sodium atom density (9×10^{11} cm^{-3}) have both been substantially raised ($C = 4.5 \times 10^3$ here); however, the collisional-broadening rate is still low, corresponding to 0.5 Torr Ar. We note that the peak heights no longer show the hyperfine structure; in this regime saturation of the transition is the principal cause of cavity transmission. In order to give some idea of the amount of saturation we note that the expected power broadening by the effective mean field for the *profile peaks* is 4 GHz (full width) at larger detunings, and 1 GHz (full width) for the central peak. This effective mean field yields $y \cong 190$ for these data. The power broadening at the profile peaks is sufficient to partially mask the inhomogeneous contributions to the structure, but hyperfine optical pumping still plays a role under these

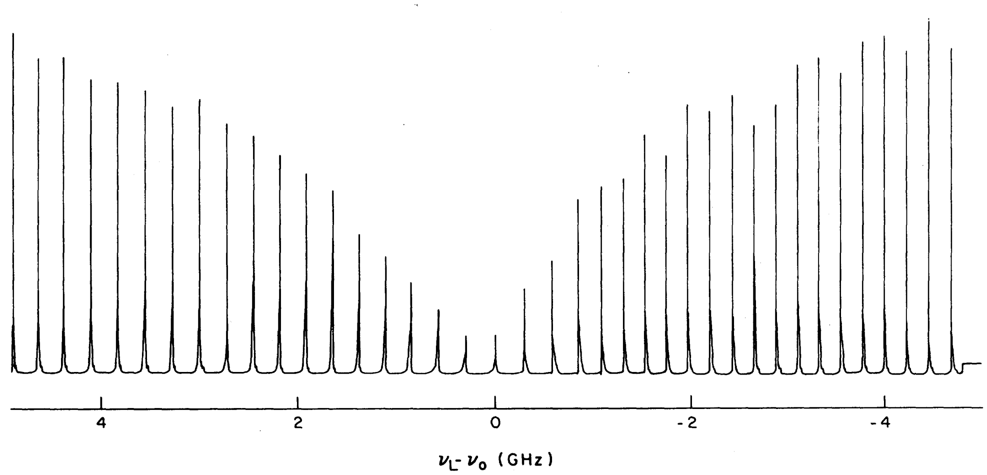

FIG. 3. Transmitted cavity power as a function of laser frequency for Na density of 9.1×10^{11} cm^{-3} and constant laser power (60 mW), illustrating dispersive bistability. The Ar pressure is 0.5 Torr and the homogeneous width $2\gamma_\perp$ is 20 MHz. The laser frequency is scanned from negative to positive detuning. Zero detuning is identified by the near symmetrical profile of small height.

conditions. There is a residual asymmetry of the peak-height distribution in Fig. 3 which has the opposite sign to that due to hyperfine structure. This is explained on the basis of optical-bistability hysteresis. A further indicator for the presence of optical bistability is the marked asymmetry of individual profiles in Fig. 3. Profiles in the negative detuning region have sharp steps on the right, whereas profiles in the positive laser detuning region have sharp steps on the left. (Zero laser-atom detuning is identified with the nearly symmetric profile of low height at the center.)

This bistability is dispersive in character, since it arises principally through saturation of the atomic sodium refractive index, which changes toward unity as the cavity power rises. Absorptive bistability is not seen in Fig. 3 (at zero laser detuning), nor is it expected for this strongly inhomogeneously broadened regime.[3,5,11,17] Note that switching is seen in the region of the two detunings (+1.4 and −1.0 GHz), where hyperfine optical pumping does not alter the index of refraction. The switching at these two detunings is clearly dispersive in character, and the smooth behavior of the observed switching versus detuning around these regions confirms that optical pumping is largely masked by saturation for these experimental conditions.

To indicate a regime where optical pumping is important, we show in Fig. 4 data taken at comparable sodium density (7.5×10^{11} cm^{-3}), but higher laser power (220 mW) and higher buffer gas pressure (4.7 Torr), where the Na confinement time is increased to ~20 times the radiative lifetime. Corresponding values of parameters are $C \simeq 700$, $y = 150$, and $\gamma_\perp = 52$ MHz. Optical-bistability hys-

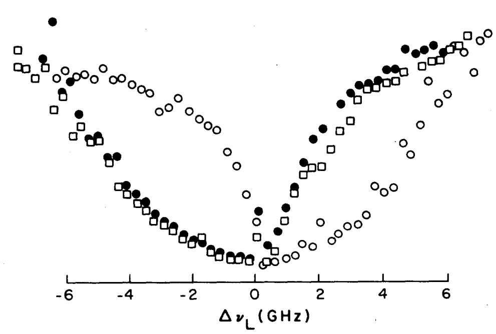

FIG. 4. Transmitted cavity power as a function of laser frequency, illustrating strong bistability hysteresis and effects of optical pumping. The Na density is 7.5×10^{11} cm^{-3}. Open circles: laser power 210 mW, laser frequency scanned left to right, Ar pressure 4.7 Torr; squares: laser power 230 mW, laser frequency scanned right to left, Ar pressure 4.7 Torr; closed circles: laser power 250 mW, laser frequency scanned right to left, Ar pressure 2 Torr.

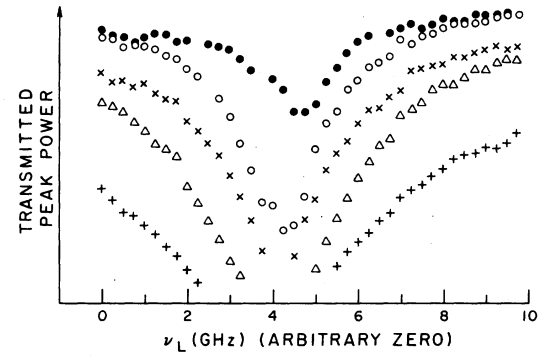

FIG. 5. Transmitted cavity power as a function of laser frequency, illustrating broadening of the transition and decrease in saturation as Ar pressure is raised. The Na density is 2×10^{11} cm^{-3} and the laser power is 26 mW. Ar pressure has the following values: dots, 2 Torr; circles, 4 Torr; crosses, 10 Torr; triangles, 22 Torr; pluses, 80 Torr.

teresis is much greater in this figure than in Fig. 3. In the large detuning region (>4 GHz) the transmission will be mainly due to saturation-based dispersive bistability, since optical-pumping effects are very small for these large detunings. However, the region of small detuning (<2 GHz) clearly reflects complex behavior which has to do with a combination of Δn due to optical pumping at low cavity powers[3] and Δn of opposite sign due to saturation at higher cavity power. The balance between these as a function of detuning determines the details of switching, which we will not examine quantitatively.

One way to achieve a single, homogeneous line is to collisionally broaden the sodium D_1 line until the broadened (homogeneous) width greatly exceeds the inhomogeneous width. Under these conditions the nuclear and electronic angular momenta are effectively decoupled and the transition loses its hyperfine structure. Figure 5 illustrates

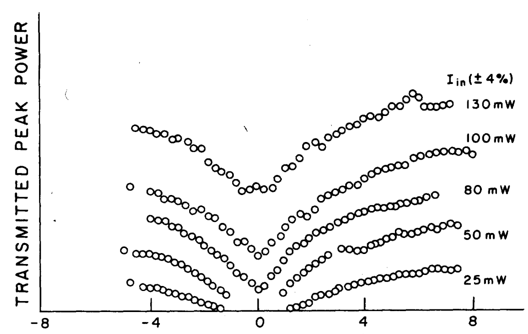

FIG. 6. Peak heights of transmitted cavity power as a function of laser frequency illustrating onset of saturation as laser power is increased. Na density 1.8×10^{11} cm^{-3}, Ar pressure 80 Torr.

the change in peak-height spectrum as the Ar pressure is increased from 2 to 80 Torr (Na density 2×10^{11} cm^{-3}, power 26 mW). The broadening of the transition and a pressure shift are apparent. Hyperfine pumping, which accounts for the absence of hyperfine structure in the lowest Ar pressure data, is not expected to be predominant at high pressures. Also, we see, as expected, that the level of saturation decreases with increasing Ar pressure (and hence $\gamma_\perp$). The critical laser power needed to obtain bistability is proportional to $\gamma_\perp$, and we could not observe optical bistability at Ar pressures much above 40 Torr ($\gamma_\perp = 400$ MHz, full homogeneous width = 800 MHz) even at our highest laser power. Consequently, to demonstrate absorptive bistability we have used 20- and 45-Torr Ar, with the former yielding $\gamma_\perp = 200$ MHz and power broadening by the effective field of 7 GHz for the unloaded cavity at cavity peaks. These data are presented in Sec. V B.

Figure 6 shows transmission curves (peak-height spectra) taken for various laser powers at 80-Torr buffer gas pressure and for a value of sodium density (1.8×10^{11} cm^{-3}) for which the

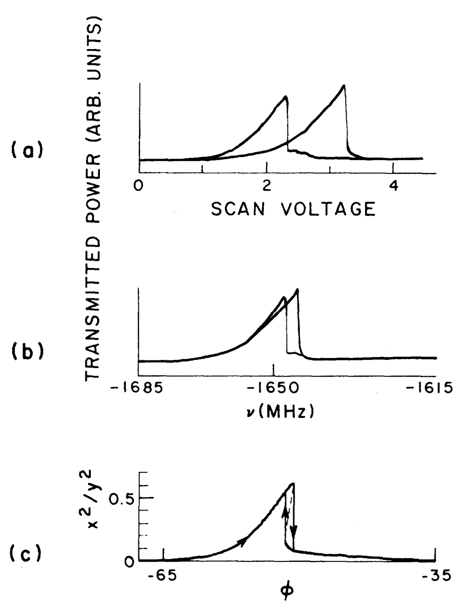

FIG. 7. Dispersive-optical bistability of the transmission peak at laser detuning at −1.65 GHz (Fig. 3), observed with a 100-MHz up-down scan. Experimental parameters are the same as for Fig. 3. (a) Oscilloscope trace of transmitted cavity power as a function of laser-frequency-drive voltage. (b) Trace corrected for laser frequency-drive hysteresis. (c) Theoretical curve [from Eq. (1)] of x^2/y^2 as a function of laser detuning ϕ from the empty cavity peak transmission. Parameters are $C = 4.5\times10^3$, $y = 65$, and $\Delta = -165$ at the profile maximum. The dotted portion of the profile gives the unstable part of the analytic curve of x^2/y^2 vs ϕ.

vapor transmits at the highest power but is opaque at lower power. The absence of hysteresis in these curves confirms that optical bistability is not achieved at the available power for this buffer gas pressure. The expected power broadening by the effective mean field at profile peaks is 40 GHz for the unloaded cavity and 130-mW laser power; this becomes 6 GHz for the smallest peak-height powers in Fig. 6. Optical-pumping effects on profile peaks are quite small at this Na density and with this degree of homogeneous broadening. Thus, all of these peak heights can be considered in terms of the TMH model and we will make a quantitative comparison in Sec. V C.

B. Dispersive and absorptive transmission profiles

An expanded view of the dispersive bistability profile at −1.65 GHz in Fig. 3 is shown in Fig. 7. The actual oscilloscope trace, taken with linear up-down frequency sweeps, is shown in Fig. 7(a), while Fig. 7(b) reproduces this trace with the laser-frequency-drive hysteresis removed. The remaining hysteresis is due to the bistability. In Fig. 7(c) we show a (TMH-model) theoretical profile obtained from Eq. (1) with $C = 4.5\times10^3$, $y = 65$, ϕ varied from −65 to −35, and Δ at profile peak equal to −165. This value of C is obtained from the known finesse and the Na density times L calculated from the cell temperature as described in Sec. V A. This Δ is obtained using $\gamma_\perp = 10$ MHz, half from the natural radiative decay and half from collisional broadening. This particular detuning (−1.65 GHz) is close to a frequency where optical pumping causes no change in index of refraction, but inhomogeneous broadening is still important for these experimental conditions. A value of 65 has been chosen for y to optimize the fit to this particular profile (different values of y would be needed to fit other peak profiles). The effective-mean-field y value [Eqs. (A1), (A5), and (A6)] is 190 at the beam waist; comparison of these y values is deferred to the conclusions section.

For Ar pressures ≥ 20 Torr, optical pumping and hyperfine structure are sufficiently masked by the homogeneous and power broadening so that the line centroid can be identified from the position of the only symmetric Fabry-Perot profile of low peak height. The height of this central peak is also independent of scan direction, when the bistability threshold is exceeded, whereas the dispersively bistable peaks on either side have unequal heights due to hystersis and these heights reverse with scan direction. Thus, although Ar collisions shift the line relative to isolated Na, the centroid of this shifted line is easily identified. When the cavity length is adjusted slightly to exactly center the

Fabry-Perot pattern, the central peak profile is determined essentially entirely by absorption. (We remember that $\gamma_\perp \gg$ empty cavity half-width.) This central profile is non-Lorentzian, with the distortion arising from nonlinearity in the D_1 absorption coefficient. The latter partially saturates with increasing cavity power, allowing the cavity power to further increase. When the feedback associated with these processes is sufficiently great the cavity power becomes multiple valued and absorptive bistability results for the center peak.

Absorptive bistability is observed at 20- and 45-Torr buffer gas pressures. Figure 8 shows oscilloscope traces of the central peak with 20-Torr Ar and high laser power (135 mW). The two profiles are taken under virtually identical conditions; the laser power for the profile on the left is just above threshold for bistability, whereas for the profile on the right (displaced on account of laser drive hysteresis) the laser power is just below threshold. Note the asymmetry in the slope on either side of the larger peak; this is consistent with expected switching hysteresis. Figure 8 also shows for comparison theoretical profiles from Eq. (1) for the cases $C=5$, $y^2=37.62$ (just above threshold), and $C=5$, $y^2=37.61$ (just below threshold). However, this value of C, chosen for best fit of the ratio of pedestal-to-peak height ratio, is substantially different from the value expected ($C=110$) from the sodium density measurements and buffer gas pressure. This "best-fit" value of y ($y\sim 6$) can be compared to the effective-field value of 70 at the beam waist.

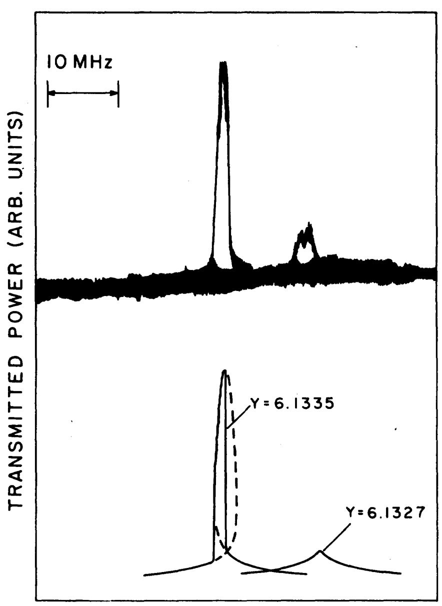

FIG. 8. Absorptive-optical bistability of the profile at the center of the line at an Ar pressure of 20 Torr. The sodium density is 4.5×10^{11} cm^{-3}. At the top is an oscilloscope trace of transmitted cavity power as a function of laser frequency for constant incident power (~135 mW). For the profile on the left, the scan is right to left and the laser power is marginally above threshold, while for the profile on the right the scan is left to right and the laser power is marginally below threshold. Below are theoretical profiles from Eq. (1), with $C=5$. The profile on the left is drawn for $y^2=37.62$, the one on the right has $y^2=37.61$, and Δ is zero at profile maximum. The peak value of x^2/y^2 is 0.32 for the left and 0.04 for the right profiles. The dotted portion of the profile gives the unstable portion of the analytic curve of x^2/y^2 vs ϕ, while the solid line corresponds to a right-to-left scan.

Discussion of these parameter comparisons is deferred to the conclusions. Absorptive bistability was also observed at 45-Torr Ar with ~200-mW laser power. This was observed as rapid switching between a pedestal and an intensity some 15 times greater, with the switching transient too rapid to expose the photograph. These data are not reproduced here, as it is felt that small power fluctuations in this critical threshold region cause severe distortions in the data. The cell temperature yields $C=70$, and the effective-field value of y is 50 for these data.

C. Comparison with plane-wave theories

As noted in Sec. V A, for 80-Torr Ar the pressure broadening (1.6 GHz) and expected power broadening (6–40 GHz) at the Fabry-Perot peaks reduce the Na D_1 transition to effectively a two-level homogeneous line. The available laser power is then below the level at which significant bistability hysteresis is observable. According to the TMH model, the Fabry-Perot profile peaks x_p^2 are given by Eq. (1), with ϕ equal to $2C\Delta/(1+\Delta^2+x^2)$ (this assumes, as is the case for the 80-Torr

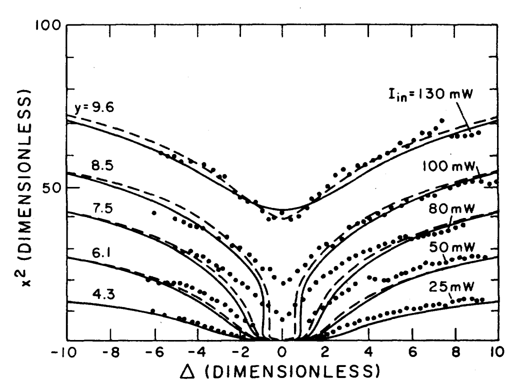

FIG. 9. Experimental peak Fabry-Perot profile heights (dots) from Fig. 6 compared with predictions from the plane-wave envelope equations. Solid curves for Eq. (4) and dashed curves for Eq. (5). $\Delta=10$ corresponds to approximately 8-GHz detuning.

data, that $d\Delta/d\phi \ll 1$):

$$y^2 = x_p^2\left(1+\frac{2C}{1+\Delta^2+x_p^2}\right)^2 . \tag{4}$$

Predictions from this "envelope" equation are compared with the data in Fig. 9. The value of C used ($C=10$) is obtained from Eq. (2) for the experimental conditions, whereas the value of y^2 is obtained from Eq. (3) using $B=113$. This B value is chosen to optimize the fit to the 130-mW data; it should be compared to the expected mean-field value of around 800, based on the discussions below Eq. (3).

This B scaling factor is constant in Fig. 9; the proportionality of y^2 with laser power has been preserved. We see from comparison of observed and calculated profile heights that the TMH theory with a *constant* scaling factor B fails even if the value of B is adjusted to obtain a fit for one power, i.e., when the incident power is raised, saturation on resonance is observed to set in more slowly than predicted on the basis of the TMH model.

The presence of standing waves in the cavity is known to have an effect on saturation of the two-level transition.[17-21] Following Ref. 18, we find that within the mean-field limit and stationary atom approximation

$$y^2 = x^2\left(\left\{1+\frac{2C}{x^2}\left[1-\left(\frac{1+\Delta^2}{1+\Delta^2+2x^2}\right)^{1/2}\right]\right\}^2 + \left\{\phi-\frac{2C\Delta}{x^2}\left[1-\left(\frac{1+\Delta^2}{1+\Delta^2+2x^2}\right)^{1/2}\right]\right\}^2\right).$$

This yields the following envelope equation for peak profile height:

$$y^2 + x_p^2\left\{1+\frac{2C}{x_p^2}\left[1-\left(\frac{1+\Delta^2}{1+\Delta^2+2x_p^2}\right)^{1/2}\right]\right\}^2 . \tag{5}$$

This is shown as a dashed curve in Fig. 9, where a fit has been made to the data, again using $C=10$, but with a y^2 scale factor of $B=97$ in Eq. (3). A minor improvement and more gradual bistability onset is obtained, but the data are still in severe disagreement (in the region of small detuning where bistability is expected from the model but does not occur experimentally).

In an attempt to explore this failure we have treated C as a free parameter (even though its value is known), but we have been unable, with either of the above models, to find any combination of fitted C and B that gives overall agreement. (Although any one data set at constant laser power may be fitted with a choice of C and B, the values differ with laser power.)

D. Comparison with Gaussian wave theory

One of the most significant differences between this experiment and the assumptions of the TMH theory is the Gaussian transverse intensity distribution in our cavity. The expression for the saturated coefficient will involve an averaging over a range of values of x^2, and this should clearly soften the onset of saturation. We now have available a quantitative investigation of the effect of the Gaussian power envelope in the regime where self-focusing and defocusing are small.[22] An independent calculation for the ring-cavity case has also now been reported by Drummond.[23] The equation for Fabry-Perot profile peak heights from Ref. 22 is

$$y^2 = x_p^2\left(1+\frac{4C}{x^2}\ln\left\{\frac{1}{2}\left[\left(\frac{1+\Delta^2+2x_p^2}{1+\Delta^2}\right)^{1/2}+1\right]\right\}\right)^2 . \tag{6}$$

The condition for small beam reshaping through focusing or defocusing is given as[22] $1-R < 3.5 \times 10^{-3} L/z_0$. For our experiments $L/z_0 \simeq 3$, giving $1-R \lesssim 10^{-2}$ which is approximately satisfied. Therefore we shall apply Eq. (6) to our results.

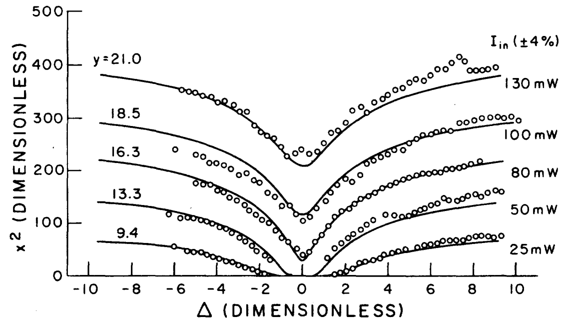

FIG. 10. Experimental peak Fabry-Perot profile heights (dots) from Fig. 6 compared with predictions from the Gaussian wave, standing-wave envelope equation, Eq. (6). Na density is 1.8×10^{11} cm^{-3}, and Ar pressure is 80 Torr. $\Delta=10$ corresponds to approximately 8-GHz detuning.

In Fig. 10 we have plotted the same experimental peak heights as in Fig. 9, and taking the expected value of $C=10$, have chosen $B=540$ to optimize the fit of Eq. (6) to the data. This compares to $B=1550$ for the axial field expected from the discussions below Eq. (3).

Agreement between the Gaussian model and the experimental data for peak heights is seen to be much better than was the case for the plane-wave models (Fig. 9). The dominant feature of the Gaussian model, compared to plane-wave models, is the much less abrupt onset of saturation at line center with increasing laser intensity. This implies that as shown in Ref. 22, absorptive bistability occurs at larger values of the cooperativity C than for the plane-wave case, and consequently the threshold laser intensities are also raised. The experimental uncertainty in B is estimated as ~50%, so that the factor of ~3 discrepancy between the actual and fitted axial y^2 is believed to be experimentally significant. Possible causes are the effects on saturation of laser fluctuations[24] and radiation trapping.[25] These are expected to be small under our experimental conditions (laser linewidth ~10% of cavity full width, Na density 2×10^{11} cm^{-3}), but they have not been examined in detail.

ACKNOWLEDGMENTS

We gratefully acknowledge valuable discussions with Professors J. Cooper and D. Walls, and we are indebted to Dr. J. Hall for assistance with the experimental arrangements. We thank Dr. R. Ballagh and Dr. D. Warrington for their helpful comments and assistance, and W. J. S. wishes to express appreciation for the hospitality accorded him at the Joint Institute for Laboratory Astrophysics, where the experiment was conducted. This work was supported in part by National Science Foundation Grant No. PHY79-04928 through the University of Colorado, and in part by the Research Committees of the University of Otago and the New Zealand University Grants Committee.

APPENDIX A

We adopt the viewpoint (Ref. 18) that atoms in the Fabry-Perot cavity are exposed to a field of magnitude appropriate to the summed intensities of the propagating and counter propagating waves (i.e., $2^{-1/2}$ of the peak field of the standing wave).

For this axially averaged intensity, the amplitude E_{CB} of the real axial sinusoidal field at the waist W_0 of a cavity empty of absorbers and on resonance with respect to linearly polarized laser radiation of power P_L is

$$E_{CB}=\left(\frac{8GP_L}{\pi W_0^2\epsilon_0 c}\right)^{1/2}, \tag{A1}$$

where the cavity gain G is the ratio of circulating cavity power (i.e., propagating in one direction) to incident laser power, and we refer to the fundamental Gaussian mode of the cavity.

The Rabi frequency corresponding to this real sinusoidal field is

$$\Omega_B=dE_{CB}/\hbar\,, \tag{A2}$$

where d is the dipole moment matrix element for π transitions between the $J=\frac{1}{2}$ lower and upper states:

$$d^2=\frac{\lambda^3\epsilon_0\hbar}{8\pi^2\tau}\,. \tag{A3}$$

Here λ is the D_1 wavelength and τ the radiative lifetime.

Finally the dimensionless input field y is defined[4] in terms of the axial field as

$$y=\frac{\Omega_B}{(\gamma_\parallel\gamma_\perp)^{1/2}}\,. \tag{A4}$$

This can thus[18] be expressed as

$$y=E_{CB}/E_S\,, \tag{A5}$$

where the saturation field is

$$E_S=\hbar(\gamma_\parallel\gamma_\perp)^{1/2}/d\,. \tag{A6}$$

In the above $\gamma_\parallel$ and $\gamma_\perp$ are longitudinal and transverse relaxation rates for the transition. In our case

$$\gamma_\parallel=\tau^{-1}=\Gamma\,,$$

and

$$\gamma_\perp=\Gamma/2+\gamma/2=\tau^{-1}(1+kP)/2\,, \tag{A7}$$

where the constant k due to pressure broadening is close to two for the Ar pressure P measured in Torr.[13]

The dimensionless transmitted field x is defined[4] as

$$x=\frac{\Omega_A}{(\gamma_\parallel\gamma_\perp)^{1/2}}\,, \tag{A8}$$

where Ω_A is the Rabi frequency encountered under the conditions of the experiment when the cavity contains absorbers and is not necessarily on resonance with respect to the laser. Since the cavity axial field at the waist E_{CA} under these conditions is given by

$$E_{CA}=\hbar\Omega_A/d\,, \tag{A9}$$

we can write x as

$$x=E_{CA}/E_S\,. \tag{A10}$$

Finally, x may be expressed in terms of the intensity I_T transmitted by the cavity by using the relation

$$E_{CA}=\left(\frac{8I_T}{\pi W_0^2\epsilon_0 c T_2}\right)^{1/2}, \tag{A11}$$

where T_2 is the transmission coefficient of the output cavity mirror.

Equations (A1) and (A11) refer to the axial fields, while the entire field at the waist varies as $\exp(-r^2/W_0^2)$ in the off-axis dimension r. There is an unavoidable ambiguity in deriving a mean field for this intensity distribution, but we will adopt the definition such that the mean field is constant across a diameter $2W_0$ and the power in the mean field is the same as that in the Gaussian mode. The result is that the mean field is $2^{-1/2}$ times the axial field, and the parameters x and y

of the mean-field model are $2^{-1/2}$ times the axial values.

With the above expressions [Eqs. (2), (A5), and (A10)] for C, y, and x, and under the constant field approximation, Eq. (1) can be shown[26] to apply to a linear focusing cavity with absorber confined to length L at the waist (size W_0) region provided the following limits apply.

The mean-field limit:

$$1-(R_1R_2)^{1/2}T\to 0\,,$$
$$\alpha L\to 0\,, \tag{A12}$$
$$\alpha L/(1-R_1^{1/2}R_2^{1/2}T)\to\eta\,,$$

where η is a finite number.

The finite detuning limit:

$$(\omega_{\text{laser}}-\omega_{\text{cavity}})/(c/2l)\to 0\,, \tag{A13}$$
$$(\omega_{\text{laser}}-\omega_{\text{cavity}})/[(1-R_1^{1/2}R_2^{1/2}T)^{1/2}(c/2l)]\to\beta\,,$$

where β is a finite number. In the above R_1, R_2 are the reflectivities (which may be unequal) of the input and output end mirrors, an intracavity loss $(1-T)$ is included, and the cavity length is l. The empty cavity gain and finesse are given by

$$G=(1-R_1)/(1-R_1^{1/2}R_2^{1/2}T)^2 \tag{A14}$$

and

$$F=\pi(R_1R_2T)^{1/2}/(1-R_1^{1/2}R_2^{1/2}T)\,. \tag{A15}$$

APPENDIX B

We suppose that laser radiation connects only $3^2S_{1/2}$ and $3^2P_{1/2}$ states (which we abbreviate a and b, respectively). Collisional transfer between $3^2P_{1/2}$ and $3^2P_{3/2}$ (state c) and collisional broadening of the ab optical transition arise through Na-buffer gas collisions. Hyperfine structure is ignored, as discussed earlier.

Because of the spherical symmetry of the collisional processes and radiative decay, it is appropriate to express the density matrix in terms of irreducible tensor components $\rho_q^k(a)$, $\rho_q^k(b)$, $\rho_q^k(c)$ for the a,b,c states, and $\rho_q^k(ab)$ for the ab optical coherence. The relevant equations of motion for π polarized excitation $E\cos\omega_L t$ can be written (in the rotating-wave approximation) with inhomogeneous broadening dominated by homogeneous broadening and time dependence of the electric field removed by transformation to the rotating frame[27]:

$$\dot\rho_0^0(a)=\Gamma\rho_0^0(b)+\sqrt{2}\,\Gamma\rho_0^0(c)-\frac{id_{ab}E}{\hbar 2\sqrt{6}}[\rho_0^1(ab)-\rho_0^{1*}(ab)]\,, \tag{B1a}$$

$$\dot\rho_0^0(b)=-(\Gamma+\gamma_t)\rho_0^0(b)+\tfrac{1}{2}\gamma_t\sqrt{2}\,\rho_0^0(c)+\frac{id_{ab}E}{\hbar 2\sqrt{6}}[\rho_0^1(ab)-\rho_0^{1*}(ab)]\,, \tag{B1b}$$

$$\dot\rho_0^0(c)=-(\Gamma+\tfrac{1}{2}\gamma_t)\rho_0^0(c)+\tfrac{1}{2}\gamma_t\sqrt{2}\,\rho_0^0(b)\,, \tag{B1c}$$

$$\dot\rho_0^1(ab)=-(i\Delta\omega+\gamma_\perp)\rho_0^1(ab)+\frac{id_{ab}E}{\hbar 2\sqrt{6}}[\rho_0^0(b)-\rho_0^0(a)]\,. \tag{B1d}$$

In Eqs. (B1), the detuning $\Delta\omega$ is $\omega_L-\omega_a$, d_{ab} is the reduced dipole matrix element between a and b states (related to the matrix element d for π transitions by $d=d_{ab}/\sqrt{6}$), $\gamma_\perp$ is as defined previously, and γ_t is the rate of collisional transfer from b to c (assumed independent of Zeeman substates). Detailed balance requires the reverse rate $(c\to b)$ to be $\sim\frac{1}{2}\gamma_t$. [Factors of $\sqrt{2}$ appear multiplying $\rho_0^0(c)$ in Eqs. (B1) from normalization of $\rho_0^0(a)$, $\rho_0^0(b)$, and $\rho_0^0(c)$.]

Solving for the steady-state expression for the optical coherence, we obtain

$$\rho_0^1(ab)=-\frac{(2\Gamma/\gamma_\perp)^{1/2}(\Delta+i)x}{1+\Delta^2+x^2(1+\gamma_t/\Gamma)/(1+\frac{3}{2}\gamma_t/\Gamma)}\,. \tag{B2}$$

In Eq. (B2), we have used the dimensionless quantities

$$\Delta=\frac{\Delta\omega}{\gamma_\perp} \tag{B3}$$

and

$$x=\frac{(d_{ab}/\sqrt{6})E}{\hbar(\Gamma\gamma_\perp)^{1/2}}=\frac{dE}{\hbar(\gamma_\perp\Gamma)^{1/2}}\,. \tag{B4}$$

We note that Eq. (B4) is consistent with Eq. (A10), provided E is understood to mean E_{CA} (the mean-field amplitude experienced by atoms in the cavity).

Equation (B2) leads to the standard result for the susceptibility for an equivalent two-state system (see, e.g., Ref. 10)

$$\chi=\frac{\alpha C}{\omega_L}\,\frac{i-\Delta}{1+\Delta^2+x_t^2}\,, \tag{B5}$$

where

$$x_t^2=x^2(1+\gamma_t/\Gamma)/(1+\tfrac{3}{2}\gamma_t/\Gamma)\,. \tag{B6}$$

This justifies the use of the two-state model for our three-level case.

The effective saturation parameter, x_t, reduces simply to x in the limit $\gamma_t\ll\Gamma$, where collisional transfer can be ignored. At high buffer gas pressure, where $\gamma_t\gg\Gamma$, we find

$$x_t^2=\tfrac{2}{3}x^2\,. \tag{B7}$$

Thus, the single consequence of rapid collisional transfer between the $P_{1/2}$ and $P_{3/2}$ states, which occurs at the higher buffer gas pressures, is the reduction of the value of B [Eq. (3)] to $\frac{2}{3}$ of its previous value.

*On leave at the Joint Institute for Laboratory Astrophysics, where the experiment was performed.

†Quantum Physics Division, National Bureau of Standards.

[1]For a history of optical bistability, see, for example, H. M. Gibbs, S. L. McCall, and T. N. C. Venkatesan Optics News 5, 6 (1979) and references therein.

[2]V. N. Lugovoi, Kvantovaya Elektron. (Moscow) 6, 2053 (1979) [Sov. J. Quantum Electron. 9, 1207 (1979)].

[3]H. M. Gibbs, S. L. McCall, and T. N. C. Venkatesan, Phys. Rev. Lett. 36, 1135 (1976); S. L. McCall, H. M. Gibbs, G. G. Churchill, and T. N. C. Venkatesan, Bull. Am. Phys. Soc. 20, 636 (1975).

[4]R. Bonifacio and L. A. Lugiato, Opt. Commun. 19, 172 (1976); Phys. Rev. A 18, 1129 (1978).

[5]R. Bonifacio and L. A. Lugiato, Lett. Nuovo Cimento 21B, 517 (1978).

[6]Some features of the model had been previously introduced in A. Szöke, V. Daneau, J. Goldhar, and M. A. Kurnit, Appl. Phys. Lett. 15, 376 (1969).

[7]For preliminary accounts of some of the work presented here see Refs. 15 and 16.

[8]R. Bonifacio and L. A. Lugiato, Lett. Nuovo Cimento 21B, 505 (1978).

[9]P. Meystre, Opt. Commun. 26, 277 (1978).

[10]The mean-field approximation was also used for dispersive bistability in Ref. 3.

[11]S. S. Hassan, P. D. Drummond, and D. F. Walls, Opt. Commun. 27, 480 (1978).

[12]G. P. Agrawal and H. J. Carmichael, Phys. Rev. A 19, 2074 (1979).

[13]D. G. McCartan and J. M. Farr, J. Phys. B 9, 985 (1976); R. H. Chatham, A. Gallagher, and E. L. Lewis, *ibid.* 13, L7 (1980).

[14]R. Seiwert, Ann. Phys. (N.Y.) 18, 54 (1956); J. Pitre and L. Krause, Can. J. Phys. 45, 2671 (1967).

[15]W. J. Sandle, R. J. Ballagh, and A. Gallagher, in *Optical Bistability, Proceedings of the International Conference on Optical Bistability, June, 1980*, edited by C. M. Bowden, M. Cistan, and H. R. Robl (Plenum, New York, 1981), p. 93.

[16]R. J. Ballagh, J. Cooper, and W. J. Sandle, J. Phys. B (to be published).

[17]S. L. McCall, Phys. Rev. A 9, 1515 (1974).

[18]G. P. Agrawal and H. J. Carmichael, Opt. Acta 27, 651 (1980).

[19]P. D. Drummond, Ph.D. thesis, University of Waikato 1979 (unpublished).

[20]S. L. McCall and H. M. Gibbs, Opt. Commun. 33, 335 (1980).

[21]R. Roy and M. S. Zubairy, Opt. Commun. 32, 163 (1980); Phys. Rev. A 21, 274 (1980).

[22]R. J. Ballagh, J. Cooper, M. W. Hamilton, W. J. Sandle, and D. M. Warrington, Opt. Commun. (in press).

[23]P. D. Drummond, IEEE J. Quantum Electron. QE-17, 301 (1981).

[24]P. Zoller, Phys. Rev. A 20, 2420 (1979).

[25]J. M. Salter, D. D. Burgess, and N. A. Ebrahim, J. Phys. B 12, L759 (1979).

[26]W. J. Sandle, in *Laser Physics, Proceedings of the Second New Zealand Summer School in Laser Physics* (Academic, New York, 1980), p. 225.

[27]These equations are generalizations of those in M. Ducloy, Phys. Rev. A 8, 1844 (1973), to include collisional coupling to a third state.